

Contents lists available at ScienceDirect

Chemosphere

journal homepage: www.elsevier.com/locate/chemosphere



Review

Applications of MXene-based membranes in water purification: A review



Yasir A.J. Al-Hamadani ^a, Byung-Moon Jun ^b, Michelle Yoon ^c, Nader Taheri-Qazvini ^{d, e}, Shane A. Snyder ^{f, g}, Min Jang ^h, Jiyong Heo ^{i, *}, Yeomin Yoon ^{b, **}

- ^a Directorate of Construction and Building, Ministry of Higher Education and Scientific Research of Iraq, 52 Street, Al-Rusafa, Baghdad, 00964, Iraq
- b Department of Civil and Environmental Engineering, University of South Carolina, Columbia, 300 Main Street, SC, 29208, USA
- ^c Department of Biology, University of Pennsylvania, Philadelphia, PA, 19104, USA
- ^d Department of Chemical Engineering, University of South Carolina, Columbia, SC, 29208, USA
- ^e Biomedical Engineering Program, University of South Carolina, Columbia, SC, 29208, USA
- f School of Civil & Environmental Engineering, Nanyang Technological University, 1 Cleantech Loop, 637141, Singapore
- g Department of Chemical and Environmental Engineering, University of Arizona, Tucson, AZ, 85721, USA
- h Department of Environmental Engineering, Kwangwoon University, 447-1, Wolgye-Dong Nowon-Gu, Seoul, Republic of Korea
- ⁱ Department of Civil and Environmental Engineering, Korea Army Academy at Young-cheon, 495 Hogook-ro, Kokyungmeon, Young-Cheon, Gyeongbuk, 38900, Republic of Korea

HIGHLIGHTS

- Performance of MXene-based membrane was reviewed for liquid separation and water purification.
- MXene-based membranes enhanced water flux and antifouling during membrane filtration.
- Valuable information was provided for applications of MXene-based membranes in water industry.
- Areas of future research for MXene-based membranes were suggested.

ARTICLE INFO

Article history: Received 20 February 2020 Received in revised form 13 April 2020 Accepted 15 April 2020 Available online 16 April 2020

Handling Editor: Shane Snyder

Keywords: MXenes Membrane Water purification Liquid separation

ABSTRACT

Since MXenes (a new family of two-dimensional materials) were first produced in 2011, they have become very attractive nanomaterials due to their unique properties and the range of potential industrial applications. Numerous recent studies have discussed the environmental applications of different MXenes in adsorption, catalysis, and membranes. Only a limited number of MXene-based membrane studies have been published to date, and most have discussed only specific MXenes (i.e., $Ti_3C_2T_x$), a small number of solutes (e.g., dyes and inorganic salts), and laboratory-scale short-term experiments under limited water-quality and operational conditions. In addition, to our knowledge, there has been no review of MXene-membrane studies. It is therefore essential to assess the current status of understanding of the performance of these membranes in liquid separation and water purification. Here, a comprehensive literature review is conducted to summarize the current preparation techniques for MXene-based membranes and their applications, particularly in terms of environmental and industrial applications (e.g., water treatment and organic solvent filtration), and to direct future research by identifying gaps in our present understanding. In particular, this review focuses on several key factors, including the effects of preparation techniques on membrane properties, operational conditions, and compound properties that influence liquid separation during MXene-based membrane filtration.

© 2020 Elsevier Ltd. All rights reserved.

^{*} Corresponding author.

^{*} Corresponding author.

Contents

1.	Introduction							
2.	Preparation techniques for MXene-based membranes 2							
	Liquio	Liquid separation performance of various MXene-based membranes						
	3.1. Water purification							
		3.1.1.	Flux and removal	5				
			Membrane properties and operating conditions					
	3.2.	Organi	c solvent filtration	9				
		3.2.1.	Flux and removal	9				
		3.2.2.	Membrane properties and operating conditions	. 11				
4.	Concl		nd areas of future study					
	Declaration of competing interest							
	Ackno	owledge	ments	. 13				
	Refer	ences		. 13				

1. Introduction

Due to industrialization and urbanization, global water consumption has increased quickly over the last five decades (Dong et al., 2017). Water pollution has also increased, mainly due to human activities and inappropriate management of natural water resources (Bhatnagar et al., 2015). For example, numerous recent studies have shown that synthetic contaminants of emerging concern can be found at very low levels (sub 1 μ g/L) in wastewater influents/effluents and raw/finished drinking water around the world (Snyder et al., 2003, 2007; Yoon et al., 2010). Different traditional and advanced treatment processes have been employed in water and wastewater treatment plants to treat both conventional and emerging pollutants, including coagulation/flocculation/ sedimentation/filtration (Joseph et al., 2013; Westerhoff et al., 2005), chlorination (Li et al., 2019a), ozonation (Westerhoff et al., 2005), carbon/nanomaterial adsorption (Joseph et al., 2011; Jung et al., 2015), membranes (Heo et al., 2011; Kim et al., 2018), and ultrasonication (Al-Hamadani et al., 2016; Im et al., 2015). Of these, membrane processes have been widely used in water and wastewater treatment in recent years (Ang et al., 2015).

Among conventional liquid-separation processes such as evaporation, distillation, crystallization, and filtration, membrane separation has become a promising technology in the past few decades in response to environmental and energy challenges (Koros and Zhang, 2017). Membrane separation and purification have been extensively employed in the chemical, pharmaceutical, and water industries and provide a range of benefits including a reduced carbon footprint, high reliability, simple operation, and reduced secondary pollution (Li et al., 2017). However, membrane separation processes are frequently inhibited by a trade-off between membrane flux and selectivity. To resolve this issue, several studies have investigated fabrication of novel membranes incorporating various nanomaterials such as carbon nanotubes (Li et al., 2019b; Yin et al., 2019), graphene oxides (Chu et al., 2016, 2017a), metalorganic frameworks (Hua et al., 2019; Liu et al., 2019b), and MXenes (Han et al., 2017; Wei et al., 2019).

Since MXenes (titanium carbide $(Ti_3C_2T_x)$, a new family of two-dimensional materials) were first produced by Drexel University researchers in 2011 (Naguib et al., 2012b), they have become very attractive nanomaterials due to their unique properties, including outstanding stability, large surface area, high electrical/thermal conductivity, excellent oxidation resistance, and hydrophilicity (Lukatskaya et al., 2013; Zhong et al., 2016). Numerous recent studies have investigated environmental applications of different MXenes in adsorption (Jun et al., 2020a; Jun et al., 2020b), catalysis

(Jun et al., in review), and membranes (Kang et al., 2017; Liu et al., 2020). For membrane applications, the ideal design criteria of membrane fabrication imply that MXene-based membranes should provide efficient separation and safe long-term operation, and environmentally friendly manufacturing processes, which are significantly influenced by the stability, dispersibility, and hydrophilicity of MXenes.

Only a limited number of MXene-based membrane studies (approximately 20 journal articles) have been published to date, and therefore evaluation of the current understanding of the performance of MXene-based membranes in liquid separation is required. The main objectives of this study were to assess the current findings on preparation techniques for these membranes and their applications, particularly in terms of their environmental and industrial applications (*e.g.*, water treatment and organic solvent filtration), and to direct future research by recognizing gaps in our present understanding. In particular, this review focuses on several key factors, including the effects of preparation on MXenebased membrane properties, operational conditions, and compound properties that influence liquid separation during MXenebased membrane filtration.

2. Preparation techniques for MXene-based membranes

Several recent studies have investigated the synthesis of multilayered MXene flakes and nanomaterials (Anasori et al., 2017; Naguib and Gogotsi, 2015; Naguib et al., 2014), including via wet etching with HF (Naguib et al., 2012a; Ren et al., 2016; Tang et al., 2012), HCl-LiF (Chen et al., 2018a; Couly et al., 2018; Fu et al., 2018), or HCl-NaF (Liu et al., 2017). Fig. 1 shows a timeline of MXene fabrication from 2011 to 2019. In common with other nanomaterial-based membranes that contain carbon nanotubes, graphene oxides, and/or metal-organic frameworks, there are three fabrication methods for membranes: (i) MXenes are used as skeleton materials for the fabrication of a lamellar-structure; (ii), different additives or other nanomaterials are added to fabricate mixed matrix membranes with MXenes; and (iii) MXenes are employed as coating materials to modify a membrane support layer. Fig. 2 shows schematics of the different methods of fabrication of MXene-based membranes supported on various materials such as anodic aluminum oxide, polyvinylidene fluoride, and polycarbonate.

A new type of lamellar membrane was fabricated using a stack of two-dimensional ${\rm Ti}_3{\rm C}_2{\rm T}_{\rm X}$ MXene nanosheets (Ding et al., 2017). Two-dimensional MXene powder was produced by etching an Al layer from ${\rm Ti}_3{\rm AlC}_2$ particles with HF, since interlayer binding is



Fig. 1. Timeline of MXenes: from Ti₃C₂ discovery to ordered divacancies modified from (Alhabeb et al., 2017).

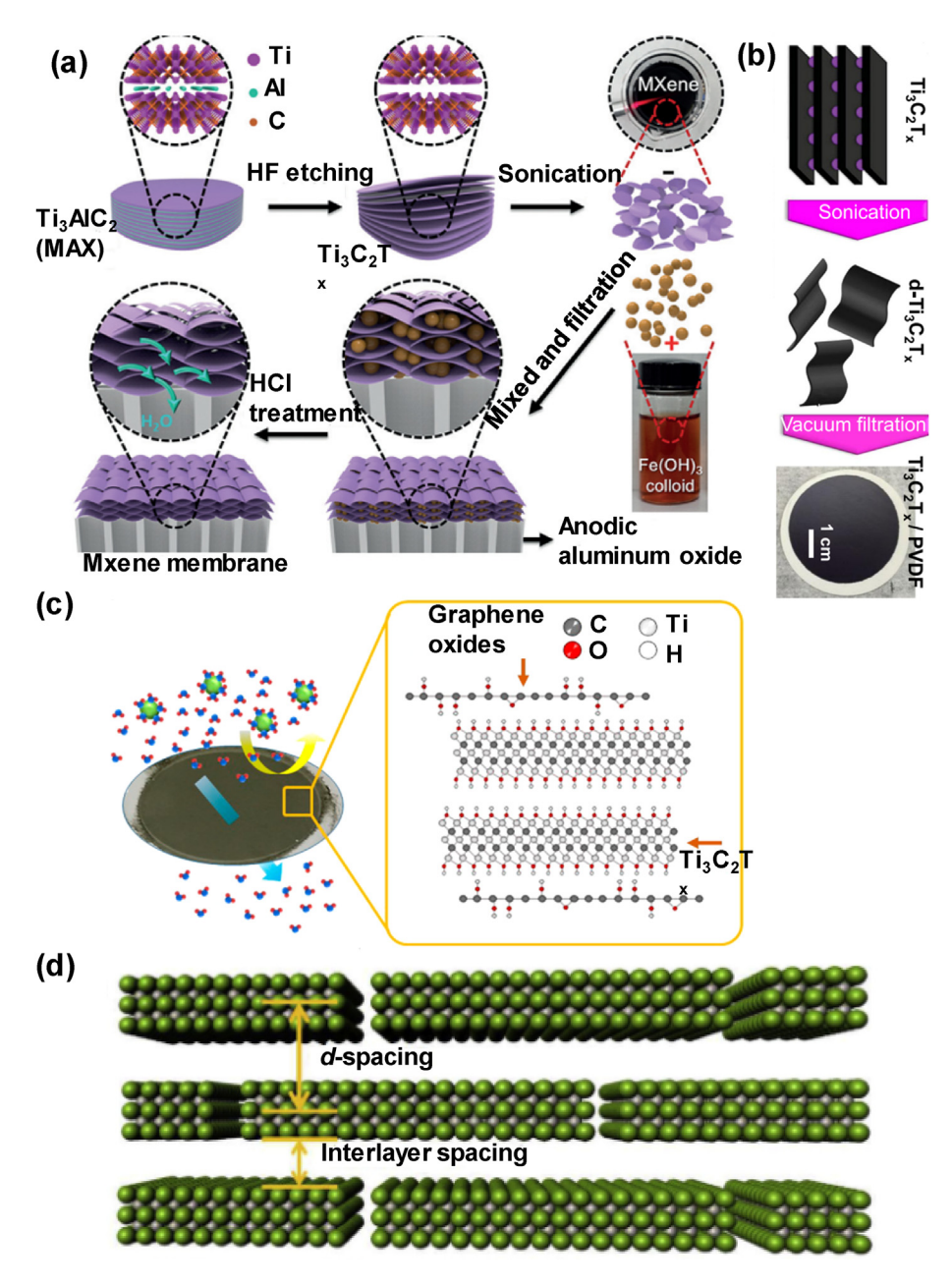


Fig. 2. Fabrication schematic of (a) MXene membrane supported on anodic aluminum oxide (Ding et al., 2017), (b) MXene membrane supported on polyvinylidene fluoride (Rasool et al., 2017), (c) MXene-GO membrane supported on polycarbonate (Kang et al., 2017), and (d) *d*-spacing and interlayer spacing between the two adjacent MXene nanosheets in the membrane (Sun et al., 2019).

weakened by removing Al as AlF₃. MXene nanosheets were fabricated by exfoliation with ultrasonication, then mixing with Fe(OH)₃ colloidal solutions to fabricate an MXene membrane by filtering on an anodic aluminum oxide membrane with a pore size of $0.2 \mu m$. Then, the Fe(OH)₃ colloids were completely removed by dissolving in HCl, which produced more flow channels for H₂O molecules, as shown in Fig. 2a. Several characterizations were conducted to verify successful fabrication of MXene membranes (Ding et al., 2017): Xray diffraction patterns to confirm the conversion of Ti₃AlC₂ to Ti₃C₂T_x, scanning/transmission electron microscopy (SEM/TEM) images to confirm the change of Ti₃AlC₂ to Ti₃C₂T_x MXene nanosheets, atomic force microscopy (AFM) to confirm the thickness (2 nm) and size distribution (100-400 nm) of MXene nanosheets; and Fourier transform infrared spectroscopy and X-ray photoelectron spectroscopy to confirm that the MXene surfaces had -F, -OH, and -O functional groups. A somewhat similar method was employed to fabricate a two-dimensional Ti₃C₂T_x MXene membrane via a facile phase-conversion technique by filtrating Ti₃C₂T_x on a polyethersulfone ultrafiltration membrane with a nominal molecular weight cutoff of 10,000 Da (Han et al., 2017). In a separate study, Rasool et al. fabricated MXene membranes by filtrating Ti₃C₂T_x nanoparticles on a polyvinylidene difluoride membrane with a pore size of 450 nm, which had antimicrobial properties for Escherichia coli (E. coli) and Bacillus subtilis (B. subtilis) (Rasool et al., 2017). The membranes were fabricated with various thicknesses $(0.6-1.8 \mu m)$ by depositing/coating 2-6-mg Ti₃C₂T_x nanosheets on a 47-mm diameter polyvinylidene difluoride substrate. While the polyvinylidene difluoride substrate was hydrophobic based on a water contact angle of 81°, the Ti₃C₂T_x nanoparticle coated membrane became very hydrophilic based on a contact angle of 37°.

Traditional uncross-linked polyamide membranes fabricated through non-solvent-induced phase inversion are somewhat unstable in organic solvents such as methanol, acetone, isopropanol, and n-heptane, as well as in oxidants such as chlorine (Anadao and Wiebeck, 2019). Han et al. employed Ti₃C₂T_x to fabricate an MXene mixed-matrix membrane with unique properties of high hydrophilicity, selectivity, and solvent resistance (Han et al., 2019). Ti₃C₂T_x nanoparticles were introduced into a polyimide (P84) polymer matrix cross-linked with triethylenetetramine to enhance the selectivity and solvent resistance. Characterization based on SEM showed that the polyimide/MXene mixed-matrix membrane had a channel size of approximately 200 nm with potential for mass transfer. Both membrane surface roughness and thickness decrease with increasing MXene content, since the active top layers of the MXene membrane become denser with increasing MXene loading. Modification of the cross-sectional structure of the membrane can be caused by more rapid interchange of H2O molecules and the solvent in the phase-inversion technique due to the hydrophilicity of MXene (Kusumawati et al., 2016). Thin-film nanofiltration membranes may be candidates for solvent filtration, since functionalization of the film filler stage instead of the polymer matrix is anticipated to produce the preferred functionality and reduce unnecessary swelling (Xue et al., 2016). An MXene-based membrane incorporated with 2% unfunctionalized Ti₃C₂T_x nanosheets on a resistant thin-film nanofiltration support enhanced the flux of isopropanol (30% increase; 3.35 L m $^{-2}$ \hat{h}^{-1} bar $^{-1}$), while the flux of other solvents (butanone, ethyl acetate, and *n*-heptane) was not improved by the membrane (Wu et al., 2016). Functionalized $Ti_3C_2T_X$ nanosheets with $-NH_2$, -COOR, $-C_6H_6$, and $-C_{12}H_{26}$ functional groups synthesized by attaching organo-functional siloxanes were incorporated on a polyacrylonitrile ultrafiltration membrane support, which significantly influenced the solvent flux for n-heptane, toluene, isopropanol, and ethyl acetate and the removal of polyethylene glycol.

The majority of current commercially available membrane

materials such as polyvinylidene fluoride, polysulfone, or polypropylene are hydrophobic, which has a negative effect on water flux and separation effectiveness, which is in turn associated with severe membrane fouling, particularly for oil/water separation membranes (Rana and Matsuura, 2010). A flexible Ti₃C₂T_x membrane was fabricated for effective treatment of oily wastewater (Saththasivam et al., 2019). During the fabrication process, a simple coating method was employed with MXene ink (2000 mg L⁻ dispersed homogeneously after pretreatment with sonication. The MXene composite membrane was fabricated by coating MXene nano-flakes on commercially available white print paper as a support using vacuum filtration. The MXene membrane appeared to be very flexible, based on SEM analyses, since the loaded configurations of the MXene coating allowed the composite membrane to bend without cracking or breakdown. In addition, AFM analyses demonstrated that the roughness of the MXene membrane (200 nm) was much smaller than that of the original printer paper substrate (914 nm), indicating reduced membrane fouling after coating with MXene. Contact analysis also showed that an MXene membrane is highly hydrophilic and oleophobic with water (almost zero within a few seconds) and with underwater oil (137°), respectively. In particular, the rapid water wetting behavior is presumably related to MXene's great attraction towards -OH groups and interlaced porous nanosheets (Han et al., 2017).

Similar to other two-dimensional nanomaterials such as graphene oxides, solute transport within MXene-based laminar membranes can take place through pores on MXene sheets, inplane pores, and/or inter-galleries between MXene sheets (Shen et al., 2016). Nevertheless, it is somewhat problematic to tune these laminar structures precisely, particularly when assuming defect-free and well-ordered two-dimensional nano-channels. Liu et al. successfully fabricated free-standing two-dimensional Ti₂CT_x MXene membranes by intercalating hyperbranched polyethyleneimine on an anodic aluminum oxide substrate (pore size = 100 nm) for effective solvent dehydration (Liu et al., 2019a). While well-ordered assembling structures of the MXene coatings were seen, limited non-selective in-plane pores were still observed in the membrane, which could negatively affect membrane performance (Shen et al., 2018). Therefore, to enhance membrane quality further, a simple interfacial polymerization technique was employed to seal potential non-selective defects using trimesoly chloride to react with the hyperbranched polyethyleneimine initially used in the membrane (Liu et al., 2019a). In a separate study, MXene-derived membranes were fabricated by depositing a Ti₂CT_x dispersion on the inner surface of an α-Al₂O₃ tubular substrate at 1 bar and room temperature (Sun et al., 2019). A pressure filtration unit was employed to fabricate an MXene membrane with a very thin modifiable interlayer space (thickness = 100 nm) between loaded adjacent nanosheets, tunable via regulating the sintering temperature.

Incorporation of silver nanoparticles into MXenes is expected to enhance the antifouling behavior of MXene-based membranes further and to improve water permeability, as shown in other silver-nanoparticle-based membranes (Andrade et al., 2015; Koseoglu-Imer et al., 2013b; Liu et al., 2015). Padney et al. successfully fabricated silver/MXene composite membranes by self-reduction of silver nitrate to silver nanoparticles on the surface of $Ti_3C_2T_x$ nanosheets, where the MXene acted instantaneously in developing nanoparticles and as a reductant (Pandey et al., 2018). Different loadings of 0–35% silver were incorporated with the MXenes to create a 470-mm membrane on a hydrophilic polyvinylidene difluoride membrane prepared by vacuum filtration (pore size = 220 nm). Overall, less than 10 wt% loss was detected for the silver/MXene membranes during stability experiments over a wide range of temperatures (<150, 150–250, and >250 °C). The

weight loss varied depending on temperature due to (i) vaporization of absorbed and bound H_2O molecules in the composite membrane at <150 °C, (ii) decay of O-containing functional groups such as oxygen, hydroxide, and carbon dioxide at 150–250 °C, and (iii) thermal decomposition of surface chemical moieties on the MXene nanosheets at >250 °C (Pandey et al., 2018).

While numerous graphene-oxide-based membranes have been studied in liquid separation (Chu et al., 2016, 2017a, 2017b), they have often been found somewhat unstable and to disintegrate in water due to electrostatic repulsion between graphene-oxide nanoparticles (Nair et al., 2012). To overcome this issue, composite $Ti_3C_2T_x$ -graphene-oxide membranes (thickness = approximately 550 nm) were fabricated, which exhibited a synergistic effect based on solute removal and water flux (Liu et al., 2020). The MXene-graphene-oxide membranes were stacked layer by layer MXene/graphene-oxide nanosheets to create twodimensional interlayer channels for water flow. The membranes were also hydrophilic, based on water-contact angle, presumably due to the presence of various functional groups including -COOH, -OH, and epoxy groups on the graphene-oxide nanosheet surface, while the presence of relatively hydrophobic MXene may have decreased the total hydrophilicity.

In recent years, TiO₂ membranes have been widely studied for industrial developments owing to benefits such as their extraordinary hydrothermal behavior, thermal/chemical strength and catalytic properties (Kim et al., 2016). Sun et al. employed Ti₃C₂T_x and TiO₂ to fabricate mesoporous MXene-TiO₂ membranes by dipcoating nanosheets/nanoparticles on the surface of an α -Al₂O₃ hollow-fiber substrate with various mass ratios of MXene/TiO₂ (0-5 wt.%) (Sun et al., 2018). TEM results showed that the TiO₂ nanoparticles were evenly placed on the two dimensional MXene nanosheets in the mixture of the 5 wt% MXene nanosheet and TiO₂ hydrosol. Based on thermogravimetric and differential scanning calorimetry analyses, three stages of weight loss were observed arising from a range of effects: (i) The weight loss at < 200 °C was due mainly to the vaporization of water; (ii) weight loss at 200–350 °C was due mainly to thermal oxidation of hydroxyethyl cellulose and polyvinyl alcohol; and (iii) in the weight loss at 350–400 °C, an exothermal peak was observed that was associated with the emergence of anatase. Overall, the findings indicate effective fabrication of mesoporous MXene-TiO2 hollow-fiber membranes (Sun et al., 2018).

A new graphene-oxide-based membrane intercalated with TiO₂ nanocrystals was prepared via in situ H₂O₂ oxidation of Ti₃C₂T_x nanoparticles followed by vacuum filtration on a mixed cellulose ester membrane (Han and Wu, 2019). The graphene-oxide-MXene-TiO₂ membrane showed excellent permeability and removal performance compared to the pristine graphene-oxide membrane and the graphene-oxide-TiO₂ membrane. H₂O₂ oxidation enhances the production of TiO₂ nanocrystals, which allow the formation of continuous nano-channels along with the MXene sheets (Wang et al., 2018b). In a separate study, Ti₃C₂T_x-graphene-oxide membranes with a thickness of approximately 90 nm were prepared by coating the nanomaterials on a porous support via vacuum filtration (Kang et al., 2017). This fabrication method appeared to be very effective in inhibiting the transport of target solutes through interedge defects or enhancing packing. The membrane, with a lattice period of 1.43 nm, swelled in the presence of water and had an actual interlayer spacing of approximately 0.5 nm. Graphene oxides are considerably larger than Ti₃C₂T_x nanoparticles, while the weight ratio of graphene oxides is smaller than that of Ti₃C₂T_x, indicating that the key solute passage channels of Ti₃C₂T_x nanoparticles are shielded with graphene-oxide coatings (Han and Wu, 2019).

3. Liquid separation performance of various MXene-based membranes

3.1. Water purification

3.1.1. Flux and removal

Membrane permeance and selectivity are key parameters for evaluating the water-purification performance of a membrane. The two-dimensional lamellar MXene membrane supported on an anodic aluminum-oxide substrate exhibited outstanding water permeance ($>1000 L m^{-2} h^{-1} bar^{-1}$) and promising removal (>85%) of target compounds excluding [Fe(CN)₆]³: 100% for bovine serum albumin (molecular weight = $67,000 \text{ g mol}^{-1}$), 99% for gold nanoparticles (5 nm), 97% for cytochrome ($2.5 \times 3.7 \text{ nm}^2$), 93% for 5,10,15,20-tetrakis-(*N*-methyl-4-pyridyl)-21,23-H-porphyrintetratosylate (1.7 \times 1.7 nm), 90% for Evans blue (1.2 \times 3.1 nm), 85% for Rhodamine B (1.8 \times 1.4 nm), and 32% for cytochrome $(0.9 \times 0.9 \text{ nm})$, which implies that the MXene membrane had a pore diameter of approximately 2-5 nm (Ding et al., 2017). While MXene membranes exhibit good removal rates, they also maintain exceptional water permeance (e.g., approximately 1050 L m⁻² h⁻¹ bar⁻¹ for Evans blue and cytochrome). This performance arises from two effects: first, the MXene nanofragments provide more water-transport pathways compared to conventional microsized MXene sheets. Water permeability through graphene-oxide membranes can be improved by reducing the flake size of the nanoparticles and/or generating more nanochannels (Sun et al., 2014); and second, intercalated nanoparticles separate the slit pores between the MXene nanosheets, which provide greater interlayer distance and generate abundant nanochannels. Graphene-oxide membranes with nanostand channels exhibited 10-fold greater water permeability than pristine graphene-oxide membranes while maintaining comparable removal rates (Huang

Ti₃C₂T_x was used to fabricate an MXene-coated membrane associated with a hydrophobic polyvinylidene difluoride membrane, which was used for the first time in a solar-assisted direct contact membrane distillation process (Tan et al., 2018). In addition to lowering the heating requirement, the degree of membrane fouling of the MXene-coated membrane was evaluated using feed water containing 200 mg L⁻¹ bovine serum albumin and 10,000 mg L⁻¹ NaCl. Under conditions with and without visiblelight irradiation, the MXene-coated membrane showed flux decreases of approximately 7-8%, significantly smaller than that of a polyvinylidene difluoride membrane (18-19%). The enhanced fouling resistance may be attributed to several effects: hydrophilic repulsion between Ti₃C₂T_x and bovine serum albumin, smaller electrostatic repulsion between Ti₃C₂T_x and bovine serum albumin, and absorption of bovine serum albumin within the Ti₃C₂T_x coating. The results showed that a Ti₃C₂T_x coating facilitated both limited heating under visible light conditions and reduced organic fouling (Tan et al., 2018).

A graphene-oxide-MXene-TiO₂ membrane exhibited approximately 7.5- and 2.5-fold higher water permeability (90 L m⁻² h⁻¹ bar⁻¹) than a pristine graphene-oxide membrane and a graphene-oxide-TiO₂ membrane, respectively (Han and Wu, 2019). Successively dispersed laminar-structure TiO₂ nanocrystals were used as intercalators, which produced homogenous nano-channels within the graphene-oxide membrane for H₂O molecule transport, while MXene loading also produced extra nano-channels for water transport. High removal rates of four dyes (Rhodamine B, methyl blue, crystal violet, and neutral red; >97%) were achieved by the graphene oxide-MXene-TiO₂ membrane; however, the removal rates of inorganic salts (61% for Na₂SO₄ and 23% for MgCl₂) were relatively low. Removal of the dyes by adsorption only was very low

(approximately <10%), implying that other mechanisms such as size exclusion and/or electro static interaction were dominant in the transport of organic dyes (Han and Wu, 2019).

Ti₃C₂T_x-graphene-oxide membranes were tested to evaluate their separation performance for various dyes (brilliant blue, rose Bengal, methylene blue, and methylene red) and inorganic salts (NaCl and MgSO₄) (Kang et al., 2017). Membrane permeance varied depending on the target compound: 2.4, 2.3, 2.1, 0.67, 0.30, and 0.23 L m⁻² h⁻¹ bar⁻¹ for MgSO₄, NaCl, methylene red, rose Bengal, methylene blue, and brilliant blue, respectively (Fig. 3a). In particular, significantly low fluxes were observed for dyes with high removal rates compared to mono-/divalent anions/cations with a small removal percentage, presumably since significant fouling by the organic dyes occurs during filtration (Van der Bruggen and Vandecasteele, 2001). The removal rates for the compounds followed the order brilliant blue (100%) ≈ methylene blue $(99.5\%) > \text{rose Bengal}(93.5\%) > \text{methylene red}(61\%) \gg MgSO_4 \text{ and}$ NaCl (<10%) (Fig. 3b). The high removal rates of dyes with different hydrated radii and charges can be attributed to size exclusion and electrostatic interaction between the membrane and compounds (Fan et al., 2017); brilliant blue (negative charge, 0.798 nm), methylene blue (positive charge, 0.504 nm), rose Bengal (negative charge, 0.588 nm), and methylene red (neutral charge, 0.487 nm). While electrostatic repulsion may occur between a negatively charged membrane and salt ions, the very low removal of ions was attributed to the interlayer spacing (0.5-0.96 nm depending on Ti₃C₂T_x swelling) being too large to sieve the ions completely. Fig. 3c shows schematic diagrams of the steric-exclusion mechanism for hydrated ions and organic dyes on the Ti₃C₂T_x-graphene oxide membrane (Kang et al., 2017).

Ti₃C₂T_x-graphene-oxide composite membranes were used to evaluate their performance based on the removal of smallmolecule organic dyes (chrysoidine G, neutral red, methylene blue, crystal violet, and brilliant blue) and two natural organicmatter types (humic acid and bovine serum albumin) (Liu et al., 2020). While the stability of graphene-oxide-based membranes is poor due to electrostatic repulsion between the nanosheet lavers (Zheng et al., 2017), the MXene-graphene-oxide membranes appeared to be very stable in water, presumably due to reduced electrostatic repulsion and increased π - π attraction. In general, the water permeance of the pristine graphene-oxide membrane was $6.5 \text{ L m}^{-2} \text{ h}^{-1} \text{ bar}^{-1}$ and membrane permeability increased with increasing incorporated MXene content (Liu et al., 2020). These findings may be explained through a number of effects: first, an increase in water flux due to an increased interlayer gap between the graphene oxide nanosheets, and second, the presence of MXene nanoparticles reducing the H-bonding interaction between H₂O molecules and O-containing functional groups of the graphene oxide nanosheets, creating enhanced water flux due to decreased resistance to water transport. Two mechanisms, size exclusion and electrostatic interaction, dominated in the transport of organic dyes in the MXene membrane, with high dependence on the properties of the target dye. The removal rate of uncharged chrysoidine G by the membrane was very high (approximately 97%), most likely due to size exclusion rather than electrostatic repulsion. However, high removal rates (~99.5%) were also observed for the other dyes, which may be attributed to both size exclusion and electrostatic interaction (attraction/repulsion) (Liu et al., 2020).

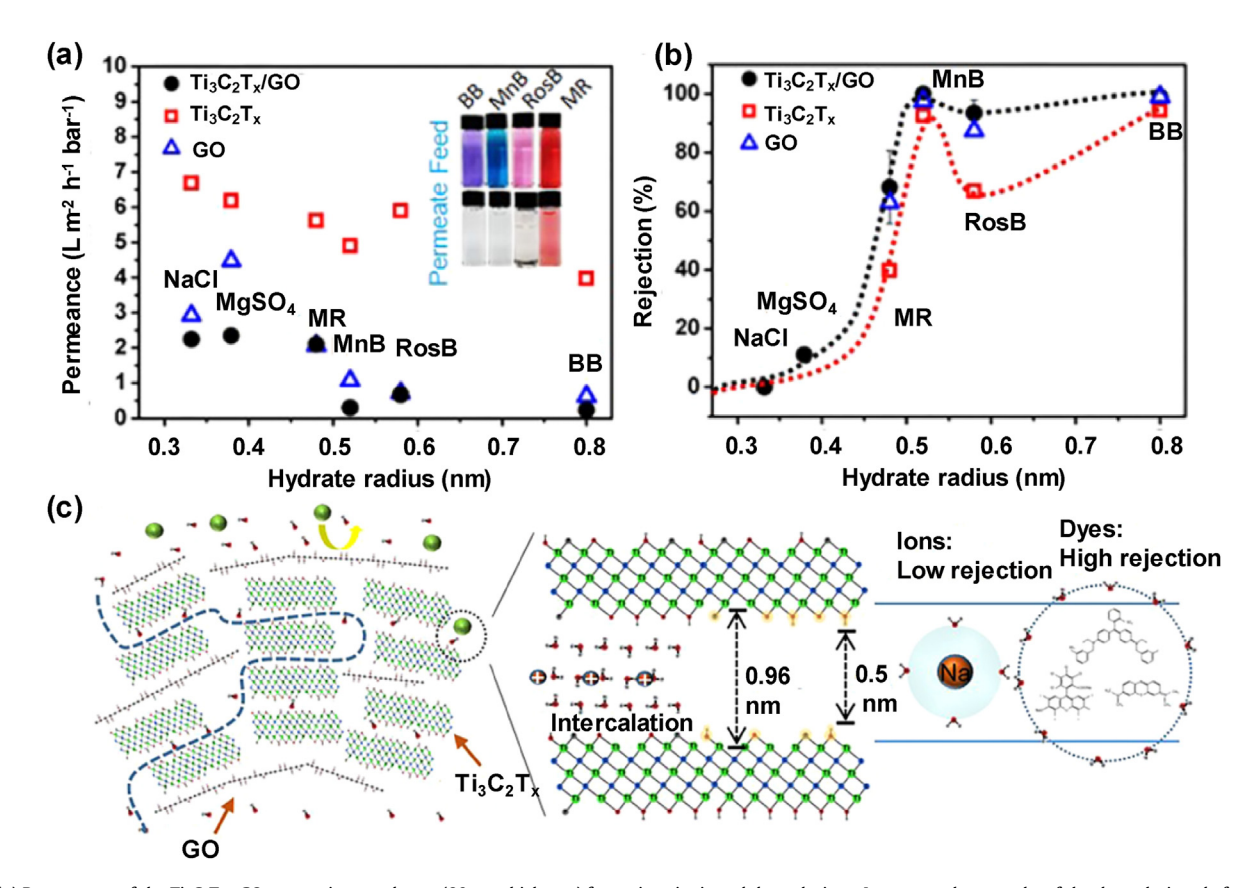


Fig. 3. (a) Permeances of the $Ti_3C_2T_x$ —GO composite membrane (90 nm thickness) for various ionic and dye solutions. Insets are photographs of the dye solutions before and after filtration. (b) Rejection of the various ionic and dye solutions indicated in (a) (MR = methyl red, MnB = methylene blue, RosB = rose Bengal, and BB = brilliant blue). (c) Schematic diagrams for the steric exclusion mechanisms for hydrated ions and dye molecules on the $Ti_3C_2T_x$ —GO membrane (Kang et al., 2017). (For interpretation of the references to colour in this figure legend, the reader is referred to the Web version of this article.)

The pure-water permeability of a 21% silver/MXene membrane with an average pore size of 2.1 nm (420 L m⁻² h⁻¹ bar⁻¹) was approximately 3.5 times greater than that of the original MXene membrane as shown in Fig. 4a (Pandey et al., 2018). In addition, the membrane showed approximately four-fold higher water flux during filtration of three organic compounds (approximately 390, 350, and 345 L m^{-2} h^{-1} bar 1 for Rhodamine B, methyl green, and bovine serum albumin, respectively) compared to the original MXene membrane, mainly due to the short transport pathway combined with extra nanopores and interlayer spaces on the hydrophilic MXene nanosheet surface (Ding et al., 2017). A silver/ MXene composite membrane also exhibited high removal of Rhodamine B (80%), methyl green (92%), and bovine serum albumin (>99%), and reasonable removal of inorganic salts of relatively small size (<1 nm) at 26, 41, and 50% for NaCl, MgCl₂, and AlCl₃, respectively (Fig. 4b). In addition, after interaction with methyl green and bovine serum albumin at 2 L of 50 mg L^{-1} of each compound, the membrane showed high flux recovery of 97% and 91%, respectively, which can be attributed to the hydrophilic property of hydrated silver nanoparticles, which enhance the resistance of the membrane surface to organic fouling (Koseoglu-Imer et al., 2013a). In general, two-dimensional nanosheets such as carbon nanotubes, metal-organic frameworks, and graphene-based membranes are fabricated by filtration-based deposition/coating on a highly porous

support (Cheng et al., 2017; Goh et al., 2013; Yang et al., 2019). The current technique forms dense films with decreased porosity, thus decreasing water permeability. However, in the silver/MXene composite membrane, silver nanoparticles produced a slit interspace (approximately 1–4 nm) between the MXene nanosheets with extra nano-pores in the silver/MXene membranes, thus improving their water permeability, as shown in Fig. 4c (Pandey et al., 2018).

A facile and scalable technique was employed to fabricate mesoporous MXene-TiO2 membranes by dip-coating the outer surface of a four-channel α -Al₂O₃ hollow-fiber substrate with a pore size of approximately 100 nm (Xu et al., 2018). The MXene-TiO₂ membranes appeared to have uneven microstructures that contained finger-like spaces and sponge-like areas, which may provide significantly less transport resistance compared to pristine hollow-fiber membrane with particle-piled pores. The performance of the MXene-TiO2 membrane was evaluated based on its permeance and removal with 3000 mg L⁻¹ dextran solution with various molecular weights of 10, 40, 70, and 500 kDa. The MXene-TiO₂ membrane (1 wt%) exhibited very high permeance of >90 L m⁻² h⁻¹ bar⁻¹ and a molecular weight cutoff of approximately 22 kDa. The permeance was one order of magnitude greater than that of a pristine hollow-fiber membrane with smaller molecular weight cutoff properties, presumably due to the elimination

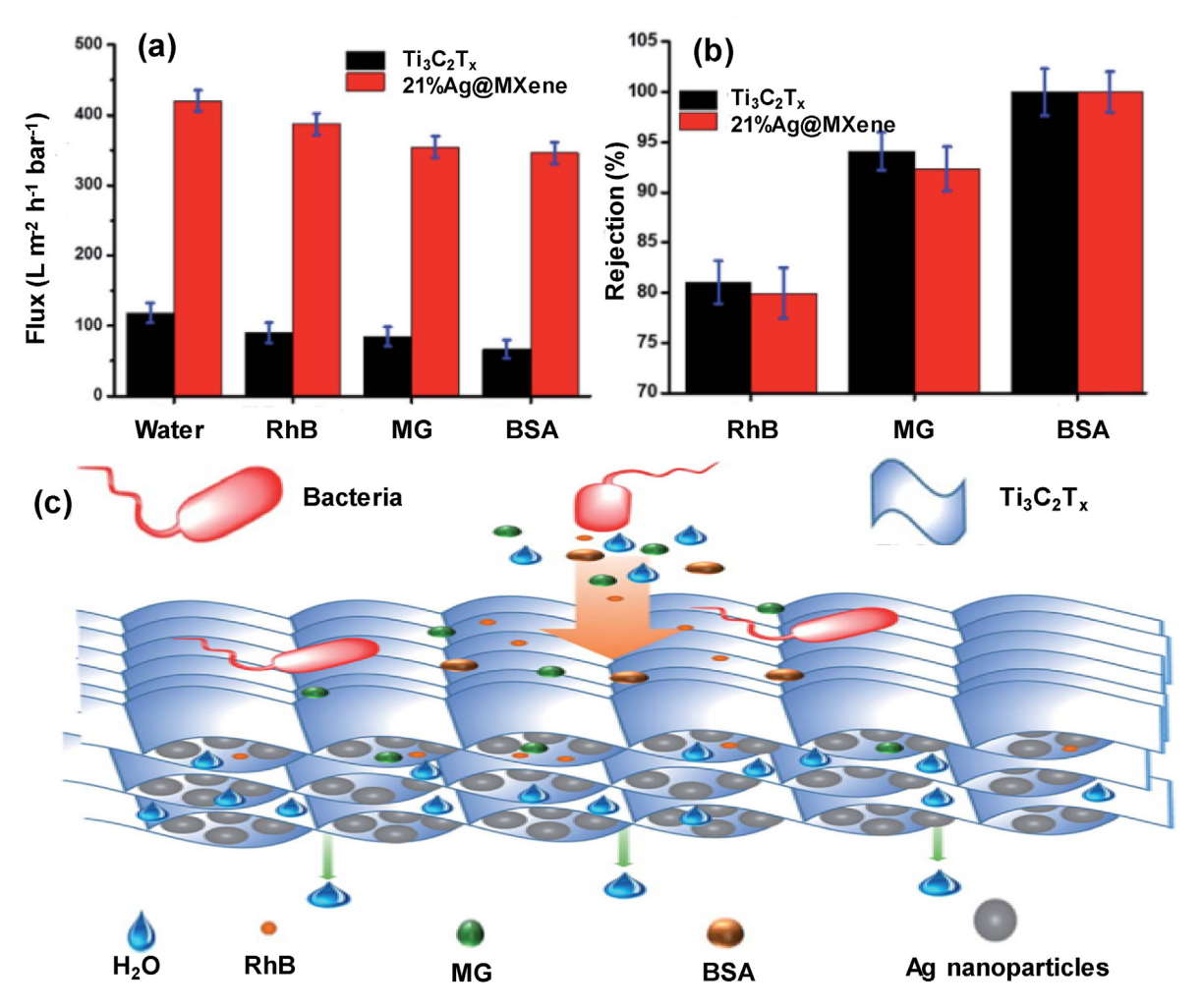


Fig. 4. Comparison of the performance of the MXene (Ti₃C₂T_x) and 21% Ag@MXene membranes for the separation of Rhodamine B (RhB), methylene green (MG), and bovine serum albumin (BSA) molecules at 25 °C: (a) flux, and (b) rejection. (c) Schematic structure and mechanisms of removal of the silver-MXene composite membrane (Pandey et al., 2018). (For interpretation of the references to colour in this figure legend, the reader is referred to the Web version of this article.)

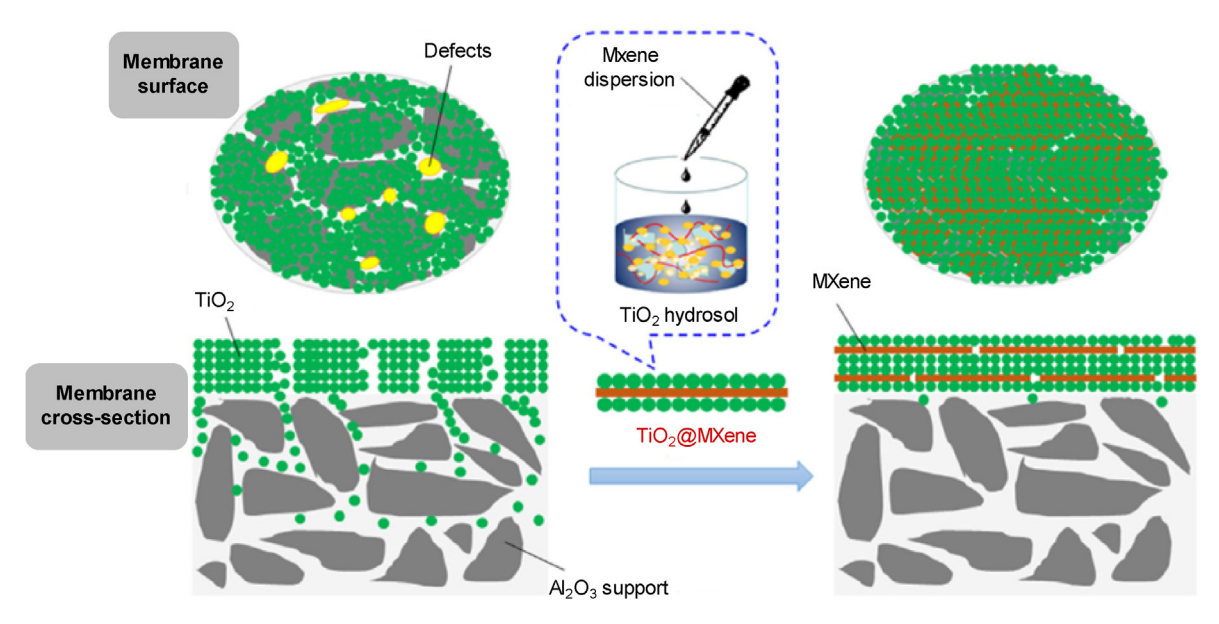


Fig. 5. Fabrication of MXene-TiO₂ membranes to remove potential defects (Xu et al., 2018).

of pinhole defects associated with the denser MXene-TiO₂ layer on the α -Al₂O₃ hollow-fiber surface (Xu et al., 2018). Fig. 5 shows the fabrication of MXene-TiO₂ membranes to remove potential defects.

Rasool et al. reported that after 24 h incubation $Ti_3C_2T_x$ -coated membranes significantly inhibited bacterial growth and decreased the viability of bacterial cells compared to the original polyvinylidene difluoride membranes (Rasool et al., 2017). High antibacterial activity against Gram-negative E. coli (73%) and Grampositive B. subtilis (67%) was observed during filtration of a Ti₃C₂T_x-modified membrane with 10⁴ CFU mL⁻¹. The primary difference in antimicrobial performance between these bacteria may have been due to differences in their cell wall configurations. For example, while *E. coli* are surrounded by a very thin peptidoglycan wall (approximately 2-3 nm) between the inner and outer cell membranes, B. subtilis contain a denser peptidoglycan layer (approximately 20-80 nm), resulting in greater resistance to the Ti₃C₂T_x coating. In addition, the lack of bacterial growth in the permeate through both the original polyvinylidene difluoride and Ti₃C₂T_x-coated membranes indicates 100% removal (Rasool et al., 2017). Since environmental conditions have a significant influence on membrane effectiveness, an initial assumption was made that membrane surface oxidation and TiO₂ formation might reduce the antibacterial behavior of the membrane surface (Gao et al., 2015). However, studies have shown that the growth inhibition of both bacteria by aged Ti₃C₂T_x-coated membranes (over 30 days) was significantly higher (>99%) than that by fresh membranes (73% for E. coli and 67% for B. subtilis). This was presumably due to the presence of TiO₂ nanoparticles on the Ti₃C₂T_x membrane surface, similar to the results of another study in which titanium substrates layered with TiO2 nanoparticles exhibited a substantial decrease in E. coli growth over large surfaces (Seddiki et al., 2014).

3.1.2. Membrane properties and operating conditions

The permeance and selectivity of a compound are considerably affected by a membrane's properties and the operating conditions. Ding et al. observed that the degree of removal of an MXene membrane varied depending on membrane thickness (Ding et al., 2017). Removal of Evans blue, cytochrome, and gold nanoparticles increased with increasing membrane thickness (95% up to 800 nm), while water molecules still passed through the relatively large

defects. However, nearly 100% removal was achieved for all compounds by a membrane with a thickness of >800 nm, presumably because the defects in the selective layer of the membrane were much smaller and therefore water molecules mainly passed through the channels between the nanosheets. The performance of the MXene membrane was also evaluated at different temperatures. Removal of Evans blue molecules using a 400 nm-thick MXene membrane increased from 83% to 90% as the transmembrane pressure was decreased from 0.6 MPa to 0.1 MPa, indicating that convection is dominant for solute transport via defects at high pressure (Ding et al., 2017).

Membrane fouling resistance and selectivity can be enhanced by modifying membrane properties such as membrane roughness, charge, and hydrophilicity (Firouzjaei et al., 2018). The performance of a MXene/polyethersulfone composite membrane was investigated based on removal and flux at a pressure of 0.1 MPa and various MXene loadings $(0-0.25 \text{ W g}^{-1})$ (Han et al., 2017). Solute removal of Congo red (92%), MgCl₂ (23%), and NaCl (14%) increased with increasing MXene loading rate, regardless of the target solute. However, the membrane flux decreased from approximately $800 \,\mathrm{L\,m^{-2}\,h^{-1}}$ (pure water) to 115 $\,\mathrm{L\,m^{-2}\,h^{-1}}$ (Congo red), 460 $\,\mathrm{L\,m^{-1}}$ h⁻¹ (MgCl₂), and 435 L m⁻² h⁻¹ (NaCl) with increasing MXene loading rate. While it was hypothesized that the hydrophilic MXene membrane might enhance membrane fouling resistance, unimproved membrane flux was observed with increasing MXene content, presumably due to an increase in mass transfer resistance (Han et al., 2017).

Lamellar MXene membranes with tunable interlayer spacing were tested using various inorganic salts (NaCl, Na₂SO₄, MgSO₄, and MgCl₂) to evaluate their water permeability and ion rejection (Sun et al., 2019). The stability of an MXene layer on α -Al₂O₃ tubular supports was found to be significantly affected by sintering at various temperatures (200, 300, 400, 450, and 500 °C). Relatively high temperatures were selected because the ceramic supports showed a weak interfacial bond at 60 °C causing severe peeling of the MXene layer on the membrane surface. In particular, the relatively weak van der Waals force and OH groups between the uneven surface of the ceramic substrate and the MXene coating were insufficient to link the support and the coatings. However, chemical interactions such as C–O–Al or Ti–O–Al between the MXene

laminates and the substrate took place at high temperatures, which improved the bond between those layers, thus leading to stable MXene membranes. The pure-water permeability of the MXene membranes first decreased and then increased with increasing temperature, being approximately 17, 15, 12, 18, and 22 L m⁻² h⁻¹ bar⁻1 at 200, 300, 400, 450, and 500 °C, respectively. However, salt removal first increased and then decreased with increasing sintering temperature, which was attributed to a decrease in the interlayer spacing of the MXene due to the defunctionalization of -OH groups associated with increasing temperature. The MXene membrane prepared at 400 °C showed the maximum ion removal of Na_2SO_4 (76%) > $MgSO_4$ (67%) > NaCl (55%) > $MgCl_2$ (46%) (Sun et al., 2019), which is proportional to the charge ratio for each cation and anion, implying that electrostatic interaction (i.e., repulsion) played a significant role in ion removal (Chen et al., 2018b).

Using a simple vacuum filtration technique, graphene oxide and MXene were incorporated to fabricate a composite lamellar membrane that showed extraordinarily fast water permeation (Wei et al., 2019). To determine the optimal ratio of Ti₃C₂T_x in the composite, water permeation and performance in removing methylene blue were evaluated for a range of MXene contents between 0 and 100 wt%. The MXene-graphene-oxide membranes exhibited a somewhat slow increase in membrane permeation (11, 19, 26, 34, and 76 L $\mathrm{m}^{-2}\,\mathrm{h}^{-1}\,\mathrm{bar}^{-1}$) for methylene blue solution with increasing MXene ratios of 0, 50, 60, 70, and 80 wt%, respectively, while a significant increase in permeation (3114 L m^{-2} h^{-1} bar⁻¹) was observed with an MXene ratio of 100 wt%. In addition and of note, removal slightly increased from 96.0 to 98.6% with increasing MXene ratios (0-70 wt%), then rapidly decreased to 73.3% and fell to nearly zero with MXene ratios of 80 and 100 wt%, respectively. These findings imply that outstanding membrane performance in terms of permeance and removal rates can be achieved by optimizing the graphene oxide and MXene loadings, which affect the appropriate interlayer spacing (Wei et al., 2019).

The performance of mesoporous MXene-TiO $_2$ membranes was found to vary significantly depending on the membrane's properties (Sun et al., 2018). Membrane surface morphology was significantly influenced by coating time: with a coating time of 1 min, the membrane surface appeared to be somewhat rough; with a coating time of 2.5 min, the membrane exhibited no noticeable pores and became smooth; and with a coating time of 5 min the membrane cracked owing to the irregular delivery of tensile stress associated with a thick membrane. Cross-sectional images showed that the membrane layer became thicker (0.79–4.96 μ m) with increasing

coating time (0.5–2.5 min, respectively), reducing pure water flux with increasing coating time. The results imply that the H₂O transport pathway through MXene-TiO₂ membranes can be increased with increasing film thickness by creating additional lamellar structures, leading to obvious longitudinal and lateral water passage routes, as shown in Fig. 6. The membrane pore sizes (6.5, 5.5, 5.3, and 5.0 nm) varied depending on the coating time (0.5, 1, 1.5, and 2 min), as estimated based on the molecular weight cutoff associated with dextran retention (21.5, 14.9, 13.9, and 12.4 kDa) (Sun et al., 2018).

3.2. Organic solvent filtration

3.2.1. Flux and removal

Functionalized MXene-based thin-film nanocomposite membranes showed various permeate fluxes depending on functional groups ($-NH_2$, -COOR, $-C_6H_6$, and $-C_{12}H_{26}$) for different solvents (n-heptane, toluene, isopropanol, and ethyl acetate) (Hao et al., 2017). Ti₃C₂T_x nanosheets enhanced isopropanol flux, but inhibited the flux of n-heptane, toluene, and ethyl acetate due to the range of affinities. In general, relatively high permeability was achieved for non-polar solvents (n-heptane and toluene; up to approximately 1.8 L m⁻² h⁻¹ bar⁻¹) compared to polar solvents (isopropanol and ethyl acetate; below approximately $0.4 \, \mathrm{L \, m^{-2} \, h^{-1}}$ bar⁻¹). The membrane flux increased slightly with increasing pressure from 4 to 10 bar, from 2.0 to 2.5 L m⁻² h⁻¹ for isopropanol and 15.8–18.7 L m⁻² h⁻¹ for *n*-heptane. The MXene membranes with C₆H₆ and C₁₂H₂₆ groups exhibited flux enhancement for nheptane (12% and 23%, respectively) compared to Ti₃C₂T_x having no functional groups, due to a strong affinity to non-polar solvents. Likewise, the presence of COOR and NH₂ functional groups enhanced the transport of isopropanol through hydrophilic MXene channels (by 11% and 19%, respectively). In addition, the most effective enhancement of solvent transport behavior for ethyl acetate, isopropanol, n-heptane and toluene on an MXene membrane was achieved by -COOR, -NH₂, -C₁₂H₂₆, and -C₆H₆ functional groups, respectively. These findings imply that incorporating functional groups into a membrane is an important method for controlling membrane transport behavior (Liu et al., 2014).

Flexible Ti₃C₂T_x membranes were evaluated for their separation performance for oil/water emulsions (Saththasivam et al., 2019). The separation efficiency of the MXene membranes was optimized by changing the MXene mass loadings coated on a white-printerpaper substrate. A test oil-in-water emulsion was obtained from sunflower oil with high viscosity, with an oil droplet size ranging

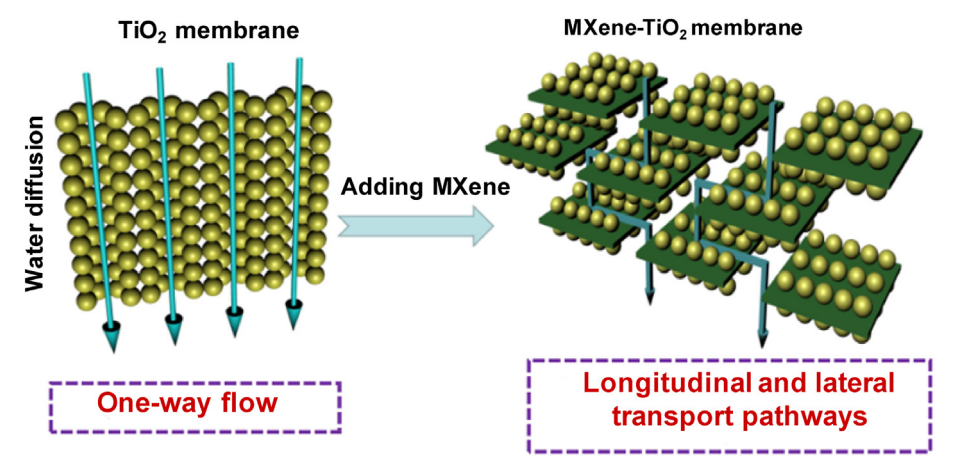


Fig. 6. Schematic of rejection mechanism: traditional one-way flow and longitudinal-lateral nanochannel model (Sun et al., 2018).

Table 1Summary of removal of selected inorganic and organic species by MXene-based membranes.

MXene	Species	Experimental condition	Support layer (pore size)	Water permeance/key removal	Key finding	Ref.
Ti ₃ C ₂ T _x	Rhodamine B Evans blue Cytochrome	$\begin{array}{l} Dead\text{-end/cross-flow} \\ C_o = 1020 \text{ mg L}^{-1} \end{array}$	Anodic aluminum oxide (200 nm)	1084 L m ⁻² h ⁻¹ bar ⁻¹ /85% (Rhodamine B) 90% (Evans blue) 97% (cytochrome)	The MXene membrane shows an outstanding water permeance (>1000 L m $^{-2}$ h $^{-1}$ bar $^{-1}$) and a high removal rate (90%) for compounds having sizes larger than 2.5 nm once applied in water treatment.	Ding et al. (2017)
	NaCl Bovine serum albumin	Cross-flow $C_0 = 10,000 \text{ mg L}^{-1}$ (NaCl); 2000 mg L ⁻¹ (bovine serum albumin)	Polyvinylidene difluoride	Flux = $\sim 10 \text{ L m}^{-2} \text{ h}^{-1}$	The MXene-coated polyvinylidene difluoride membrane conferred a 56–64% reduction in flux decline compared to the uncoated membrane. This is due to both higher electrostatic repulsion and also enhanced adsorption of bovine serum albumin by MXene.	Tan et al. (2018)
	Congo red Gentian violet MgCl ₂ Na ₂ SO ₄ NaCl	Dead-end $C_0 = 100$ -1000 mg L^{-1}	Polyethersulfone	405 L m ⁻² h ⁻¹ bar ⁻¹ /92% (Congo red) 80% (gentian violet) 2.3% (MgCl ₂) 13.2% (Na ₂ SO ₄) 13.8% (NaCl)	Owing to the MXene composite loose lamellar structure, the composite membrane could exhibit effective permselectivity in the separation of dyes from salts.	Han et al. (2017)
	E. coli B. subtilis	$C_o = \text{~~}2700 \text{ CFU mL}^{-1}$	Polyvinylidene difluoride (1200 nm)	37.4 L m ⁻² h ⁻¹ bar ⁻¹ />99% (E. coli) >99% (B. subtilis)	Surface oxidation of aged membrane presented an important enhancement of anti-microbial activity as compared with the pristine membranes.	Rasool et al. (2017)
	Oil	Glass filtration unit 1% v/v oil-in-water emulsion	Conventional print paper	$472 \text{ L m}^{-2} \text{ h}^{-1} \text{ bar}^{-1}$ with oil content/>99% (total organic carbon)	The print paper was employed as a substrate to provide mechanical flexibility and strength, and the hydrophilic MXene layer functions as a selective layer to effectively separate emulsified oil from water.	Saththasivam et al. (2019)
	Na_2SO_4 Mg_2SO_4 $MgCl_2$ $NaCl$ $VOSO_4$	$\begin{aligned} &\text{Cross-flow} \\ &\text{C}_o = 10 \text{ mM} \end{aligned}$	Tubular α -Al ₂ O ₃ (120 nm)	$5-15\ 25\ L\ m^{-2}\ h^{-1}\ bar^{-1}/50-99\%$ (VOSO ₄ \gg Na ₂ SO ₄ > Mg ₂ SO ₄ > NaCl > MgCl ₂)	The interlayer spacing of MXene-derived membranes lessened from 0.371 nm (60 $^{\circ}$ C) to 0.265 nm (450 $^{\circ}$ C). This resulted from the moisture loss and de-functionalization (-OH) occurring within the MXene film at elevated temperatures.	Sun et al. (2019)
Ti ₃ C ₂ T _x -Ag	Rhodamine B Methyl green Bovine serum albumin	$\begin{array}{l} \text{Dead-end} \\ \text{C}_{\text{o}} = 50100 \text{ mg L}^{-1} \end{array}$	Polyvinylidene difluoride (470 nm)	~420 L m ⁻² h ⁻¹ bar ⁻¹ /79.9% (Rhodamine B) 92.3% (methyl green) >99% (bovine serum albumin)	The 21% silver@MXene composite membrane exhibited enhanced bactericidal properties as validated by over 99% <i>E. coli</i> growth prevention, compared with approximately 60% for the original MXene membrane.	Pandey et al. (2018)
Ti ₃ C ₂ T _x -graphene oxide	Brilliant blue Rose Bengal Methylene blue Methylene red MgSO ₄ NaCl	Dead-end $C_o = 10 \text{ mg L}^{-1}$	Polycarbonate and nylon (20 –90 nm)	~25 L m ⁻² h ⁻¹ bar ⁻¹ /95.4 (brilliant blue) 94.6 (rose Bengal) 40 (methylene blue) 5 (MgSO ₄) <1 (NaCl)	The findings approved the composite membrane's great retention of organic dyes with hydrated radii greater than 0.5 nm which is owing to a combination of physical steric exclusion and electrostatic repulsion with $\rm Ti_3C_2T_x$ layers.	Kang et al. (2017)
	Rhodamine B Methyl blue Crystal violet Neutral red Na ₂ SO ₄ NaCl	$\begin{aligned} & \text{Dead-end} \\ & C_o = 10 \text{ mg L}^{-1} \\ & (\text{dyes}); \text{ 5 mmol L}^{-1} \\ & (\text{inorganic salts}) \end{aligned}$	Mixed cellulose ester (200 nm)	89.6 L m ⁻² h ⁻¹ bar ⁻¹ />97% (dyes) 61% (Na ₂ SO ₄) 23% (NaCl)	The obtained membrane achieved a highly enhanced water permeance of up to $89.6 \ L \ m^{-2} \ h^{-1} \ bar^{-1}$, which is approximately 7.5 times that of pristine GO membrane and 2.5 times that of GO/TiO ₂ membrane prepared via conventional methods.	Han and Wu (2019)
	Chrysoidine G Neutral red Methylene blue Crystal violet Brilliants blue Humic acid Bovine serum albumin	Dead-end $C_o = 10 \text{ mg L}^{-1}$	Mixed cellulose ester (450 nm)	71.9 L m ⁻² h ⁻¹ bar ⁻¹ />99% (dyes) 61% (Na ₂ SO ₄) 23% (NaCl)	This outstanding removal performance was attributed to the combined effects of molecular sieving, mainly, and electrostatic interaction of the composite membranes.	Liu et al. (2020)
	Methyl orange Methylene blue Acid yellow 14 Indigo carmine Eeosin	$\begin{array}{l} Dead\text{-end} \\ C_o = 10 \text{ mg L}^{-1} \end{array}$	Porous nylon membrane (220 nm)	~8.5—11 L m ⁻² h ⁻¹ bar ⁻¹ />95%	The resultant graphene oxide/MXene membranes showed very high flux for pure solvents (21.0, 48.3, 25.0, 10.8, 6.18 L m $^{-2}$ h $^{-1}$ for water, acetone, methanol, ethanol and IPA) and outstanding dyes molecular separation performance (>90%).	Wei et al. (2019)

Xu et al.	(2018)			Sun et al.	(2018)		
A crack-free TiO ₂ -MXene layer was well created on macroporous	disks by a single cycle of coating, aging, and calcination, which	could expressively simplify the process and decrees the cost of	membrane fabrication.	The prepared MXene-TiO ₂ layer showed 'ideal' pathways	(longitudinal-lateral transport nano-channel) for dextran	molecules between TiO ₂ nanoparticles and MXene nanosheets.	
$\sim 90 \text{ L m}^{-2} \text{ h}^{-1} \text{ bar}^{-1} /> 95\%$	(molecular weight, >30 kDa)			$100-140 \text{ L m}^{-2} \text{ h}^{-1} \text{ bar}^{-1}/>90\%$	(molecular weight, >20 kDa)		
a-Al ₂ O ₃ hollow	fiber (100 nm)			α -Al ₂ O ₃ hollow	fiber (300 nm)		
Dead-end	$C_{\rm o} = 3000~{ m mg}~{ m L}^{-1}$	Molecular	weight $= 10-500 \text{ kDa}$	Dead-end	$C_{ m o} = 6500~{ m mg}~{ m L}^{-1}$	Molecular	weight = 10-70 kDa
Dextran				Dextran			
x-TiO ₂							

 $\mathsf{C}_{\mathrm{o}} = \mathsf{organic}$ initial concentration

from 1 to 18 μ m (mean size = 3.9 μ m) (Gao et al., 2014). Very poor oil removal was observed for porous paper without the MXene loading, despite a maximum flux of 2720 L m⁻² h⁻¹ bar⁻¹. However, the oil removal ratio in the permeate was enhanced by 98.5% (oil content, 103 mg L^{-1} to 1.6 mg L^{-1}) with increasing MXene mass loading (0.1-0.8 mg), while the membrane flux decreased approximately five-fold (1020–204 L $\rm m^{-2}~h^{-1}~bar^{-1}$). The reduced flux and enhanced filtrate quality of the highly hydrophilic and oleophobic MXene membrane was attributed to its relatively high dense/interlaced porous structure and active layer. For an optimized MXene membrane with a mass loading of 0.4 mg, membrane flux and removal rates varied depending on the oil-in-water emulsion type, such as diesel, silicone oil, petroleum ether, hexane and sunflower oil. The permeation flux of the optimized MXene membrane was in the order hexane > petroleum ether > silicone oil > diesel > sunflower oil, while the permeation oil content followed a somewhat different order: petroleum ether < silicone oil ≤ hexane < diesel < sunflower oil. Overall, this simple MXene membrane exhibited exceptional flexibility and strength, and provided a simple method for membrane scale-up by means of MXene ink on printer paper (Saththasivam et al., 2019).

Graphene oxide-MXene composite membranes have been evaluated for their potential for organic solvent nanofiltration applications (Wei et al., 2019). Similar to an earlier study (Yang et al., 2017), membranes that incorporated only graphene oxide showed very ineffective permeance for commonly used organic solvents such as acetone, ethanol, isopropyl alcohol, and methanol. However, membranes that incorporated only MXene showed very high permeance for pure organic solvents: methanol acetone $(8900 \text{ L m}^{-2} \text{ h}^{-1} \text{ bar}^{-1}) > (3780 \text{ L m}^{-2} \text{ h}^{-1} \text{ bar}^{-1}) > \text{ ethanol}$ $(2180 \,\mathrm{L\,m^{-2}\,h^{-1}\,bar^{-1}}) > \text{isopropyl alcohol } (1060 \,\mathrm{L\,m^{-2}\,h^{-1}\,bar^{-1}}).$ While fairly similar permeance was observed even with methylene blue dissolution in these solvents, very low methylene blue removal (<2%) was observed for the MXene-only membrane. The graphene-oxide-MXene membranes exhibited both reasonably high permeance and removal of solvent-dye solutions; $36-122 \text{ L m}^{-2} \text{ h}^{-1} \text{ bar}^{-1}/90-97\%$ for acetone-methylene blue and $3.5-13.5 \text{ L m}^{-2} \text{ h}^{-1} \text{ bar}^{-1}/90-97\%$ for isopropyl alcohol -methylene blue with various MXene ratios. These differences in permeance and dye-removal rates were attributed to the effects of solvent viscosity on the interlayer spacing of the membranes. For example, an MXene-graphene-oxide membrane with an MXene ratio of 70 wt% and an interlayer spacing of 0.127 nm exhibited enlarged interlayer spacing after immersion in pure acetone (0.134 nm), isopropyl alcohol (0.143 nm), ethanol (0.145 nm), and methanol (0.149 nm) for 12 h (Wei et al., 2019).

3.2.2. Membrane properties and operating conditions

A polyimide (P84)/MXene membrane exhibited 100% removal of gentian violet dve regardless of solvent type (water, acetone, dimethylformamide, and methanol), while the solvent resistance of the membrane varied depending on the solvent type and the MXene content (Han et al., 2019). Polyimide has frequently been employed to fabricate organic solvent membranes due to its membrane-forming qualities and permselectivity (Campbell et al., 2016). The water flux of the MXene membrane clearly increased at first, from approximately 100 L m^{-2} h^{-1} to 275 L m^{-2} h^{-1} , with increasing MXene loading $(1\% \text{ Ti}_3\text{C}_2\text{T}_x)$ at a pressure of 0.1 MPa, and then decreased to approximately 175 L m⁻² h⁻¹ with an MXene loading of 2%. The flux trends can be explained as follows: homogenously lamellar MXene layers with high hydrophilicity and plentiful water nanochannels (particularly those produced by the mixture including the inorganic additive, triethylenetetramine) significantly enhance the membrane flux (Wang et al., 2018a). However, a further increase in MXene loading results in encapsulation of the MXene nanoparticles in the polymer matrix together with the formation of a sticky casting solution and a thick functional layer, which negatively influence the membrane flux (Ding et al., 2015). All MXene membranes exhibited significant flux declines for each solvent (approximately 55% for acetone, 70% for methanol, and 60% for dimethylformamide) after the MXene membrane had been soaked in the solvent for 18 days (Han et al.,

A two-dimensional defect-free MXene (Ti₂CT_x) membrane that incorporated hyperbranched polyethyleneimine and trimesoly chloride was tested for solvent dehydration, and differences in solvent flux were observed that depended on the solvent type and the solvent-to-water ratio (Liu et al., 2019a). Dehydration of organic solvents or water/organic solvent mixtures, which entails high energy consumption, has attracted increased attention owing to the extensive consumption of organic solvents in numerous industries (Mashtalir et al., 2014). The MXene membrane had a relatively high water flux (\sim 2200 L m⁻² h⁻¹) with a very small water content (12.6 wt%) during dehydration of water/methanol mixtures, while for ethanol and isopropanol dehydration, the permeate water content increased significantly to approximately 80 and 99 wt% and the water flux decreased to approximately 1400 and $1000 \text{ L m}^{-2} \text{ h}^{-1}$, respectively (Liu et al., 2019a). These findings might be attributed to the decreased molecular kinetic diameters of the solvents; 0.47 nm (isopropanol), 0.43 nm (ethanol), and 0.36 nm (methanol). Ti₂CT_x-based membranes showed better solvent dehydration performance compared with Ti₃C₂T_x-based membranes in terms of permeate water content and water flux. presumably due to sorption and steric exclusion effects. Table 1 summarizes the performance of various MXene-based membranes for the removal of selected inorganics and organics, and key findings.

4. Conclusions and areas of future study

Since MXenes were first discovered in 2011, their potential for environmental and industrial applications has been increasingly recognized. In particular, recent studies have shown that the effective fabrication of various MXenes has resulted in high potential for applications of MXene-based membranes in the area of water purification and organic solvent filtration. While there has been only a limited number of studies of MXene-based membranes in recent years, three common fabrication techniques have emerged: (i) MXenes are employed as skeleton materials for the preparation of lamellar-structure membranes; (ii) various additives or other nanomaterials such as graphene oxide and TiO2 are added to fabricate mixed-matrix membranes with MXenes; and (iii) MXenes are used as coating materials on membrane supports consisting of various materials such as anodic aluminum oxide. polyvinylidene fluoride, and polycarbonate.

Overall, MXene-based membranes have shown outstanding performance compared to pristine membranes, based on their permeance and removal qualities for inorganic and organic solutions containing organic dyes (e.g., Rhodamine B, Evans blue, cytochrome, brilliant blue, rose Bengal, methylene blue, methylene red, and etc.), inorganic salts (e.g., NaCl, Na₂SO₄, MgCl₂, and MgSO₄), or other organics (e.g., bovine serum albumin and dextran). These findings are presumably attributable to the following effects: (i) MXene nanofragments/nanosheets modified/combined with other nanomaterials, such as graphene oxide and/or TiO2 nanoparticles, provide more water transport pathways than pristine membranes; (ii0 intercalated MXene-based nanoparticles separate the pores on MXene nanosheets, increasing interlayer separation and thereby producing abundant nanochannels; and (iii) hydrophilic and negatively charged MXenes have a high capacity for incorporation of specific species/functionalities that benefit increased membrane fouling resistance and improved membrane selectivity, owing to steric exclusion, adsorption, and electrostatic interaction (i.e., both repulsion and attraction). In addition, the transport of various solvents such as ethyl acetate, isopropanol, *n*-heptane and toluene is effectively enhanced by functionalizing MXene-based membranes with different functional groups including -COOR, $-NH_2$, $-C_{12}H_{26}$, and $-C_6H_6$.

Challenges remain in improving MXene-based membranes for future applications, particularly for liquid separation and water purification. Effective development of more stable, dispersible, and hydrophilic MXenes in water is essential to fabricate efficient MXene-based membranes successfully. Comprehensive studies are necessary to develop effective MXene-based membranes particularly in terms of various crosslinkers and membrane substrates affecting membrane performance. In order to clearly understand the mechanisms of liquid separation by MXene-based membranes, evaluation of detailed molecular structure of the membrane is also necessary. Since numerous MXenes (over 70 family members) have been fabricated to date, this is a key fabrication strategy for MXenebased membranes that may provide efficient separation, safe long-

MXene-based membrane properties MXene loading

- Interlayer nano-channel size
- Hydrophilicity
- Charge
- Surface area



Liquid separation

Solvent quality or operating conditions

- рН
- Solute concentration
- Temperature
- Background inorganics
- Natural organic matter
- Membrane pressure
- Bench/pilot/full scale
- Dead-end/cross-flow

Solute physicochemical properties

- Solute molecular weight
- Solute size/geometry
- Charge/pKa
- Hydrophilicity

Fig. 7. Areas of future study of MXene-based membrane in liquid separation.

term operation, and environmentally friendly manufacturing processes. In addition, recent MXene-based membrane studies have been restricted to specific MXenes (i.e., Ti₃C₂T_x), a few solutes (e.g., dyes and inorganic salts), and laboratory-scale short-term experiments with dead-end stirred-cell units under limited water-quality and operational conditions. Thus, a complete assessment of various MXene-based membranes for various conventional and emerging contaminants (e.g., natural organic matter, endocrine-disrupting compounds, pharmaceuticals, and personal-care products) under varying water chemistry (e.g., pH, background organics and ions, and temperature) and operational (e.g., pressure and recovery) conditions is essential. In addition, a comprehensive evaluation is necessary to examine the effects of various emerging MXenes on membrane preparation and membrane properties in terms of charge, hydrophilicity, interlayer spacing, and surface smoothness, since it is challenging to evaluate the interactions between contaminants and MXene, the homogeneity of MXene dispersion in various solvents, and the development of effective incorporation methods. This information will enable measurement of large-scale and long-term membrane stability for promoting applications of MXene-based membranes. Fig. 7 shows the areas of future study of MXene-based membranes in terms of MXene-based membrane properties, solute physicochemical properties, operation conditions, and solvent/water quality conditions in liquid separation.

Declaration of competing interest

The authors declare that they have no known competing financial interests or personal relationships that could have appeared to influence the work reported in this paper.

Acknowledgements

This research was supported by the National Science Foundation, USA (OIA-1632824) and by Basic Science Research Program through the National Research Foundation of Korea (NRF) funded by the Ministry of Education, South Korea (NRF-2017R1D1A1B03031352).

References

- Al-Hamadani, Y.A.J., Chu, K.H., Flora, J.R.V., Kim, D.H., Jang, M., Sohn, J., Joo, W., Yoon, Y., 2016. Sonocatalytical degradation enhancement for ibuprofen and sulfamethoxazole in the presence of glass beads and single-walled carbon nanotubes. Ultrason. Sonochem. 32, 440—448.
- Alhabeb, M., Maleski, K., Anasori, B., Lelyukh, P., Clark, L., Sin, S., Gogotsi, Y., 2017. Guidelines for synthesis and processing of two-dimensional titanium carbide (Ti₃C₂T_X MXene). Chem. Mater. 29 (18), 7633–7644.
- Anadao, P., Wiebeck, H., 2019. Membrane: Preparation by Nonsolvent-Induced Phase Inversion. Crc Press-Taylor & Francis Group, Boca Raton.
- Anasori, B., Lukatskaya, M.R., Gogotsi, Y., 2017. 2D metal carbides and nitrides (MXenes) for energy storage. Nat. Rev. Mater. 2 (2), 16098.
- Andrade, P.F., de Faria, A.F., Oliveira, S.R., Arruda, M.A.Z., Goncalves, M.D., 2015. Improved antibacterial activity of nanofiltration polysulfone membranes modified with silver nanoparticles. Water Res. 81, 333–342.
- Ang, W.L., Mohammad, A.W., Hilal, N., Leo, C.P., 2015. A review on the applicability of integrated/hybrid membrane processes in water treatment and desalination plants. Desalination 363, 2–18.
- Bhatnagar, A., Sillanpaa, M., Witek-Krowiak, A., 2015. Agricultural waste peels as versatile biomass for water purification a review. Chem. Eng. J. 270, 244–271.
- Campbell, J., Burgal, J.D., Szekely, G., Davies, R.P., Braddock, D.C., Livingston, A., 2016. Hybrid polymer/MOF membranes for organic solvent nanofiltration (OSN): chemical modification and the quest for perfection. J. Membr. Sci. 503, 166–176.
- Chen, C., Boota, M., Urbankowski, P., Anasori, B., Miao, L., Jiang, J.J., Gogotsi, Y., 2018a. Effect of glycine functionalization of 2D titanium carbide (MXene) on charge storage. J. Mater. Chem. 6 (11), 4617–4622.
- Chen, L., Moon, J.H., Ma, X.X., Zhang, L., Chen, Q., Chen, L.N., Peng, R.Q., Si, P.C., Feng, J.K., Li, Y.H., Lou, J., Ci, L.J., 2018b. High performance graphene oxide nanofiltration membrane prepared by electrospraying for wastewater purification. Carbon 130, 487–494.
- Cheng, Q.Y., Ye, D.D., Chang, C.Y., Zhang, L.N., 2017. Facile fabrication of superhydrophilic membranes consisted of fibrous tunicate cellulose nanocrystals for

- highly efficient oil/water separation. J. Membr. Sci. 525, 1–8.
- Chu, K.H., Fathizadeh, M., Yu, M., Flora, J.R.V., Jang, A., Jang, M., Park, C.M., Yoo, S.S., Her, N., Yoon, Y., 2017a. Evaluation of removal mechanisms in a graphene oxidecoated ceramic ultrafiltration membrane for retention of natural organic matter, pharmaceuticals, and inorganic salts. ACS Appl. Mater. Interfaces 9 (46), 40369–40377.
- Chu, K.H., Huang, Y., Yu, M., Heo, J., Flora, J.R.V., Jang, A., Jang, M., Jung, C., Park, C.M., Kim, D.H., Yoon, Y., 2017b. Evaluation of graphene oxide-coated ultrafiltration membranes for humic acid removal at different pH and conductivity conditions. Separ. Purif. Technol. 181, 139–147.
- Chu, K.H., Huang, Y., Yu, M., Her, N., Flora, J.R.V., Park, C.M., Kim, S., Cho, J., Yoon, Y., 2016. Evaluation of humic acid and tannic acid fouling in graphene oxidecoated ultrafiltration membranes. ACS Appl. Mater. Interfaces 8 (34), 22270–22279.
- Couly, C., Alhabeb, M., Van Aken, K.L., Kurra, N., Gomes, L., Navarro-Suarez, A.M., Anasori, B., Alshareef, H.N., Gogotsi, Y., 2018. Asymmetric flexible MXenereduced graphene oxide micro-supercapacitor. Adv. Electron. Mater. 4 (1), 1700339.
- Ding, L., Wei, Y.Y., Wang, Y.J., Chen, H.B., Caro, J., Wang, H.H., 2017. A two-dimensional lamellar membrane: MXene nanosheet stacks. Angew. Chem. Int. Ed. 56 (7), 1825–1829.
- Ding, R., Zhang, H.Q., Li, Y.F., Wang, J.T., Shi, B.B., Mao, H., Dang, J.C., Liu, J.D., 2015. Graphene oxide-embedded nanocomposite membrane for solvent resistant nanofiltration with enhanced rejection ability. Chem. Eng. Sci. 138, 227–238.
- Dong, L., Dai, M., Liang, H.W., Zhang, N., Mancheri, N., Ren, J.Z., Dou, Y., Hu, M.M., 2017. Material flows and resource productivity in China, South Korea and Japan from 1970 to 2008: a transitional perspective. J. Clean. Prod. 141, 1164–1177.
- Fan, L., Zhang, Q., Yang, Z., Zhang, R.N., Liu, Y.N., He, M.R., Jiang, Z.Y., Su, Y.L., 2017. Improving permeation and antifouling performance of polyamide nano-filtration membranes through the incorporation of arginine. ACS Appl. Mater. Interfaces 9 (15), 13577–13586.
- Firouzjaei, M.D., Shamsabadi, A.A., Aktij, S.A., Seyedfour, S.F., Sharifian Gh, M., Rahimpour, A., Esfahani, M.R., Ulbricht, M., Soroush, M., 2018. Exploiting synergetic effects of graphene oxide and a silver-based metal-organic framework to enhance antifouling and anti-biofouling properties of thin-film nanocomposite membranes. ACS Appl. Mater. Interfaces 10 (49), 42967–42978.
- Fu, Q.S., Wang, X.Y., Zhang, N., Wen, J., Li, L., Gao, H., Zhang, X.T., 2018. Self-assembled ${\rm Ti}_3{\rm C}_2{\rm T}_x/{\rm SCNT}$ composite electrode with improved electrochemical performance for supercapacitor. J. Colloid Interface Sci. 511, 128–134.
- Gao, S.J., Shi, Z., Zhang, W.B., Zhang, F., Jin, J., 2014. Photoinduced superwetting single-walled carbon nanotube/TiO2 ultrathin network films for ultrafast separation of oil-in-water emulsions. ACS Nano 8 (6), 6344–6352.
- Gao, Y.P., Chen, H., Zhou, A.G., Li, Z.Y., Liu, F.F., Hu, Q.K., Wang, L.B., 2015. Novel hierarchical TiO₂/C nanocomposite with enhanced photocatalytic performance. Nano 10 (5), 1550064.
- Goh, K.L., Setiawan, L., Wei, L., Jiang, W.C., Wang, R., Chen, Y., 2013. Fabrication of novel functionalized multi-walled carbon nanotube immobilized hollow fiber membranes for enhanced performance in forward osmosis process. J. Membr. Sci. 446, 244–254.
- Han, R.L., Ma, X.F., Xie, Y.L., Teng, D., Zhang, S.H., 2017. Preparation of a new 2D MXene/PES composite membrane with excellent hydrophilicity and high flux. RSC Adv. 7 (89), 56204–56210.
- Han, R.L., Xie, Y.L., Ma, X.F., 2019. Crosslinked P84 copolyimide/MXene mixed matrix membrane with excellent solvent resistance and permselectivity. Chin. J. Chem. Eng. 27 (4), 877–883.
- Han, R.Y., Wu, P.Y., 2019. High-performance graphene oxide nanofiltration membrane with continuous nanochannels prepared by the in situ oxidation of MXene. J. Mater. Chem. 7 (11), 6475–6481.
- Hao, L., Zhang, H.Q., Wu, X.L., Zhang, J.K., Wang, J.T., Li, Y.F., 2017. Novel thin-film nanocomposite membranes filled with multi-functional Ti₃C₂T_x nanosheets for task-specific solvent transport. Comos. Part A-Appl. S. 100, 139–149.
- Heo, J., Joseph, L., Yoon, Y., Park, Y.G., Her, N., Sohn, J., Yoon, S.H., 2011. Removal of micropollutants and NOM in carbon nanotube-UF membrane system from seawater. Water Sci. Technol. 63 (11), 2737–2744.
- Hua, W.K., Zhang, T.H., Wang, M., Zhu, Y.D., Wang, X.F., 2019. Hierarchically structural PAN/UiO-66-(COOH)₂ nanofibrous membranes for effective recovery of Terbium(III) and Europium(III) ions and their photoluminescence performances. Chem. Eng. J. 370, 729–741.
- Huang, H.B., Song, Z.G., Wei, N., Shi, L., Mao, Y.Y., Ying, Y.L., Sun, L.W., Xu, Z.P., Peng, X.S., 2013. Ultrafast viscous water flow through nanostrand-channelled graphene oxide membranes. Nat. Commun. 4, 2979.
- Im, J.K., Yoon, J., Her, N., Han, J., Zoh, K.D., Yoon, Y., 2015. Sonocatalytic-TiO₂ nanotube, Fenton, and CCl₄ reactions for enhanced oxidation, and their applications to acetaminophen and naproxen degradation. Separ. Purif. Technol. 141, 10
- Joseph, L., Boateng, L.K., Flora, J.R.V., Park, Y.G., Son, A., Badawy, M., Yoon, Y., 2013. Removal of bisphenol A and 17 alpha-ethinyl estradiol by combined coagulation and adsorption using carbon nanomaterials and powdered activated carbon. Separ. Purif. Technol. 107, 37—47.
- Joseph, L., Heo, J., Park, Y.G., Flora, J.R.V., Yoon, Y., 2011. Adsorption of bisphenol A and 17 alpha-ethinyl estradiol on single walled carbon nanotubes from seawater and brackish water. Desalination 281, 68–74.
- Jun, B.M., Han, J., Park, C.M., Yoon, Y., 2020a. Ultrasonic degradation of selected dyes using Ti₃C₂T_x MXene as a sonocatalyst. Ultrason. Sonochem. 64, 104933.
- Jun, B.M., Park, C.M., Heo, J., Yoon, Y., 2020b. Adsorption of selected dyes on Ti₃C₂T_x

- MXene and Al-based metal-organic framework. Ceram. Int. 46, 2960–2968.
- Jun, B.M., Park, C.M., Heo, J., Yoon, Y., 2020c. Adsorption of Ba^{2+} and Sr^{2+} from model fracking wastewater by $Ti_3C_2T_x$ MXene. J. Environ. Manag. 256, 109940.
- Jung, C., Boateng, L.K., Flora, J.R.V., Oh, J., Braswell, M.C., Son, A., Yoon, Y., 2015. Competitive adsorption of selected non-steroidal anti-inflammatory drugs on activated biochars: experimental and molecular modeling study. Chem. Eng. J. 264. 1–9.
- Kang, K.M., Kim, D.W., Ren, C.E., Cho, K.M., Kim, S.J., Choi, J.H., Nam, Y.T., Gogotsi, Y., Jung, H.T., 2017. Selective molecular separation on Ti₃C₂T_x-graphene oxide membranes during pressure-driven filtration: comparison with graphene oxide and mXenes. ACS Appl. Mater. Interfaces 9 (51). 44687–44694.
- Kim, S., Chu, K.H., Al-Hamadani, Y.A.J., Park, C.M., Jang, M., Kim, D.H., Yu, M., Heo, J., Yoon, Y., 2018. Removal of contaminants of emerging concern by membranes in water and wastewater: a review. Chem. Eng. J. 335, 896—914.
- Kim, S.J., Chi, W.S., Jeon, H., Kim, J.H., Patel, R., 2016. Spontaneously self-assembled dual-layer mixed matrix membranes containing mass-produced mesoporous TiO₂ for CO₂ capture. J. Membr. Sci. 508, 62–72.
- Koros, W.J., Zhang, C., 2017. Materials for next-generation molecularly selective synthetic membranes. Nat. Mater. 16 (3), 289–297.
- Koseoglu-Imer, D.Y., Kose, B., Altinbas, M., Koyuncu, I., 2013. The production of polysulfone (PS) membrane with silver nanoparticles (AgNP): physical properties, filtration performances, and biofouling resistances of membranes. I. Membr. Sci. 428, 620–628.
- Kusumawati, N., Koestiari, T., Muslim, S., 2016. The development of a new polymer membrane: PSf/PVDF blended membrane. Res. J. Pharmaceut. Biol. Chem. Sci. 7 (4), 69–77.
- Li, C.X., Chen, C.B., Wang, Y.J., Fu, X.Z., Cui, S., Lu, J.Y., Li, J., Liu, H.Q., Li, W.W., Lau, T.C., 2019a. Insights on the pH-dependent roles of peroxymonosulfate and chlorine ions in phenol oxidative transformation. Chem. Eng. J. 362, 570–575.
- Li, K.Z., Lee, B., Kim, Y., 2019b. High performance reverse osmosis membrane with carbon nanotube support layer. J. Membr. Sci. 592, 117358.
- Li, X., Liu, Y.X., Wang, J., Gascon, J., Li, J.S., Van der Bruggen, B., 2017. Metal-organic frameworks based membranes for liquid separation. Chem. Soc. Rev. 46 (23), 7124–7144.
- Liu, F.F., Zhou, J., Wang, S.W., Wang, B.X., Shen, C., Wang, L.B., Hu, Q.K., Huang, Q., Zhou, A.G., 2017. Preparation of high-purity V₂C MXene and electrochemical properties as Li-ion batteries. J. Electrochem. Soc. 164 (4), A709–A713.
- Liu, G.Z., Shen, J., Ji, Y.F., Liu, Q., Liu, G.P., Yang, J., Jin, W.Q., 2019a. Two-dimensional Ti₂CT_x MXene membranes with integrated and ordered nanochannels for efficient solvent dehydration. J. Mater. Chem. 7 (19), 12095–12104.
- Liu, R.T., Sui, Y.M., Wang, X.Z., 2019b. Metal-organic framework-based ultrafiltration membrane separation with capacitive-type for enhanced phosphate removal. Chem. Eng. J. 371, 903–913.
- Liu, S.S., Fang, F., Wu, J.J., Zhang, K.S., 2015. The anti-biofouling properties of thinfilm composite nanofiltration membranes grafted with biogenic silver nanoparticles. Desalination 375, 121–128.
- Liu, T., Liu, X.Y., Graham, N., Yu, W.Z., Sun, K.N., 2020. Two-dimensional MXene incorporated graphene oxide composite membrane with enhanced water purification performance. J. Membr. Sci. 593, 117431.
- Liu, W.P., Hu, S., Liu, G.H., Pan, F.S., Wu, H., Jiang, Z.Y., Wang, B.Y., Li, Z.X., Cao, X.Z., 2014. Creation of hierarchical structures within membranes by incorporating mesoporous microcapsules for enhanced separation performance and stability. J. Mater. Chem. 2 (15), 5267–5279.
- Lukatskaya, M.R., Mashtalir, O., Ren, C.E., Dall'Agnese, Y., Rozier, P., Taberna, P.L., Naguib, M., Simon, P., Barsoum, M.W., Gogotsi, Y., 2013. Cation intercalation and high volumetric capacitance of two-dimensional titanium carbide. Science 341 (6153), 1502–1505.
- Mashtalir, O., Cook, K.M., Mochalin, V.N., Crowe, M., Barsoum, M.W., Gogotsi, Y., 2014. Dye adsorption and decomposition on two-dimensional titanium carbide in aqueous media. J. Mater. Chem. 2 (35), 14334–14338.
- Naguib, M., Come, J., Dyatkin, B., Presser, V., Taberna, P.L., Simon, P., Barsoum, M.W., Gogotsi, Y., 2012a. MXene: a promising transition metal carbide anode for lithium-ion batteries. Electrochem. Commun. 16 (1), 61–64.
- Naguib, M., Gogotsi, Y., 2015. Synthesis of two-dimensional materials by selective extraction. Accounts Chem. Res. 48 (1), 128–135.
- Naguib, M., Mashtalir, O., Carle, J., Presser, V., Lu, J., Hultman, L., Gogotsi, Y., Barsoum, M.W., 2012b. Two-dimensional transition metal carbides. ACS Nano 6 (2), 1322–1331.
- Naguib, M., Mochalin, V.N., Barsoum, M.W., Gogotsi, Y., 2014. 25th anniversary article: MXenes: a new family of two-dimensional materials. Adv. Mater. 26 (7), 992–1005.
- Nair, R.R., Wu, H.A., Jayaram, P.N., Grigorieva, I.V., Geim, A.K., 2012. Unimpeded permeation of water through helium-leak-tight graphene-based membranes. Science 335 (6067), 442–444.
- Pandey, R.P., Rasool, K., Madhavan, V.E., Aissa, B., Gogotsi, Y., Mahmoud, K.A., 2018. Ultrahigh-flux and fouling-resistant membranes based on layered silver/MXene (Ti₃C₂T_X) nanosheets. J. Mater. Chem. 6 (8), 3522—3533.
- Rana, D., Matsuura, T., 2010. Surface modifications for antifouling membranes. Chem. Rev. 110 (4), 2448–2471.
- Rasool, K., Mahmoud, K.A., Johnson, D.J., Helal, M., Berdiyorov, G.R., Gogotsi, Y., 2017. Efficient antibacterial membrane based on two-dimensional Ti₃C₂T_x (MXene) nanosheets. Sci. Rep. 7, 1598.
- Ren, C.E., Zhao, M.Q., Makaryan, T., Halim, J., Boota, M., Kota, S., Anasori, B., Barsoum, M.W., Gogotsi, Y., 2016. Porous two-dimensional transition metal

- carbide (MXene) flakes for high-performance Li-ion storage. Chemelectrochem 3 (5), 689–693.
- Saththasivam, J., Wang, K., Yiming, W., Liu, Z.Y., Mahmoud, K.A., 2019. A flexible Ti₃C₂T_x (MXene)/paper membrane for efficient oil/water separation. RSC Adv. 9 (29), 16296–16304.
- Seddiki, O., Harnagea, C., Levesque, L., Mantovani, D., Rosei, F., 2014. Evidence of antibacterial activity on titanium surfaces through nanotextures. Appl. Surf. Sci. 308, 275–284.
- Shen, J., Liu, G.P., Huang, K., Chu, Z.Y., Jin, W.Q., Xu, N.P., 2016. Subnanometer twodimensional graphene oxide channels for ultrafast gas sieving. ACS Nano 10 (3), 3398–3409.
- Shen, J., Liu, G.Z., Ji, Y.F., Liu, Q., Cheng, L., Guan, K.C., Zhang, M.C., Liu, G.P., Xiong, J., Yang, J., Jin, W.Q., 2018. 2D MXene nanofilms with tunable gas transport channels. Adv. Funct. Mater. 28 (31), 1801511.
- Snyder, S.A., Adham, S., Redding, A.M., Cannon, F.S., DeCarolis, J., Oppenheimer, J., Wert, E.C., Yoon, Y., 2007. Role of membranes and activated carbon in the removal of endocrine disruptors and pharmaceuticals. Desalination 202 (1–3), 156–181.
- Snyder, S.A., Westerhoff, P., Yoon, Y., Sedlak, D.L., 2003. Pharmaceuticals, personal care products, and endocrine disruptors in water: implications for the water industry. Environ. Eng. Sci. 20 (5), 449–469.
- industry. Environ. Eng. Sci. 20 (5), 449–469.
 Sun, P.Z., Zheng, F., Zhu, M., Song, Z.G., Wang, K.L., Zhong, M.L., Wu, D.H., Little, R.B., Xu, Z.P., Zhu, H.W., 2014. Selective trans-membrane transport of alkali and alkaline earth cations through graphene oxide membranes based on cation-pi interactions. ACS Nano 8 (1), 850–859.
- Sun, Y.Q., Li, S.L., Zhuang, Y.X., Liu, G.Z., Xing, W.H., Jing, W.H., 2019. Adjustable interlayer spacing of ultrathin MXene-derived membranes for ion rejection. J. Membr. Sci. 591, 117350.
- Sun, Y.Q., Xu, Z., Zhuang, Y.X., Liu, G.Z., Jin, W.Q., Liu, G.P., Jing, W.H., 2018. Tunable dextran retention of MXene-TiO₂ mesoporous membranes by adjusting the 2D MXene content. 2D Mater. 5 (4), 045003.
- Tan, Y.Z., Wang, H., Han, L., Tanis-Kanbur, M.B., Pranav, M.V., Chew, J.W., 2018. Photothermal-enhanced and fouling-resistant membrane for solar-assisted membrane distillation. J. Membr. Sci. 565, 254–265.
- Tang, Q., Zhou, Z., Shen, P.W., 2012. Are MXenes promising anode materials for Li ion batteries? Computational studies on electronic properties and Li storage capability of ${\rm Ti_3C_2}$ and ${\rm Ti_3C_2X_2}$ (X = F, OH) monolayer. J. Am. Ceram. Soc. 134 (40), 16909–16916.
- Van der Bruggen, B., Vandecasteele, C., 2001. Flux decline during nanofiltration of organic components in aqueous solution. Environ. Sci. Technol. 35 (17), 3535–3540.
- Wang, J.T., Chen, P.P., Shi, B.B., Guo, W.W., Jaroniec, M., Qiao, S.Z., 2018a. A regularly channeled lamellar membrane for unparalleled water and organics permeation. Angew. Chem. Int. Ed. 57 (23), 6814–6818.
- Wang, R.T., Wang, S.J., Zhang, Y.B., Jin, D.D., Tao, X.Y., Zhang, L., 2018b. Graphene-coupled Ti₃C₂ MXenes-derived TiO₂ mesostructure: promising sodium-ion capacitor anode with fast ion storage and long-term cycling. J. Mater. Chem. 6 (3), 1017–1027.
- Wei, S.C., Xie, Y., Xing, Y.D., Wang, L.C., Ye, H.Q., Xiong, X., Wang, S., Han, K., 2019. Two-dimensional graphene oxide/MXene composite lamellar membranes for efficient solvent permeation and molecular separation. J. Membr. Sci. 582, 414–422.
- Westerhoff, P., Yoon, Y., Snyder, S., Wert, E., 2005. Fate of endocrine-disruptor, pharmaceutical, and personal care product chemicals during simulated drinking water treatment processes. Environ. Sci. Technol. 39 (17), 6649–6663.
- Wu, X.L., Hao, L., Zhang, J.K., Zhang, X., Wang, J.T., Liu, J.D., 2016. Polymer-Ti₃C₂T_x composite membranes to overcome the trade-off in solvent resistant nanofiltration for alcohol-based system. J. Membr. Sci. 515, 175–188.
- Xu, Z., Sun, Y.Q., Zhuang, Y.X., Jing, W.H., Ye, H., Cui, Z.F., 2018. Assembly of 2D MXene nanosheets and TiO₂ nanoparticles for fabricating mesoporous TiO₂-MXene membranes. J. Membr. Sci. 564, 35–43.
- Xue, S.M., Xu, Z.L., Tang, Y.J., Ji, C.H., 2016. Polypiperazine-amide nanofiltration membrane modified by different functionalized multiwalled carbon nanotubes (MWCNTs). ACS Appl. Mater. Interfaces 8 (29), 19135–19144.
- Yang, E., Karahan, H.E., Goh, K., Chuah, C.Y., Wang, R., Bae, T.H., 2019. Scalable fabrication of graphene-based laminate membranes for liquid and gas separations by crosslinking-induced gelation and doctor-blade casting. Carbon 155, 129–137.
- Yang, Q., Su, Y., Chi, C., Cherian, C.T., Huang, K., Kravets, V.G., Wang, F.C., Zhang, J.C., Pratt, A., Grigorenko, A.N., Guinea, F., Geim, A.K., Nair, R.R., 2017. Ultrathin graphene-based membrane with precise molecular sieving and ultrafast solvent permeation. Nat. Mater. 16 (12), 1198–1202.
- Yin, C.S., Xiong, B.Y., Liu, Q.C., Li, J.J., Qian, L.B., Zhou, Y.W., He, C.Q., 2019. Lateralaligned sulfonated carbon-nanotubes/Nafion composite membranes with high proton conductivity and improved mechanical properties. J. Membr. Sci. 591, 117356
- Yoon, Y., Ryu, J., Oh, J., Choi, B.G., Snyder, S.A., 2010. Occurrence of endocrine disrupting compounds, pharmaceuticals, and personal care products in the Han River (Seoul, South Korea). Sci. Total Environ. 408 (3), 636–643.
- Zheng, S.X., Tu, Q.S., Urban, J.J., Li, S.F., Mi, B.X., 2017. Swelling of graphene oxide membranes in aqueous solution: characterization of interlayer spacing and insight into water transport mechanisms. ACS Nano 11 (6), 6440–6450.
- Zhong, Y., Xia, X.H., Shi, F., Zhan, J.Y., Tu, J.P., Fan, H.J., 2016. Transition metal carbides and nitrides in energy storage and conversion. Adv. Sci. 3 (5), 1500286.